PAN ARCHIVES OF ACOUSTICS
Vol. **39**, No. 1, pp. 103–115 (2014)

DOI: 10.2478/aoa-2014-0011

Experimental Study of Silent Sonar

Jacek MARSZAL

Department of Marine Electronic Systems
Faculty of Electronics, Telecommunications and Informatics
Gdansk University of Technology
Narutowicza 11/12, 80-233 Gdańsk, Poland; e-mail: jacek.marszal@eti.pg.gda.pl

(*received October 15, 2013; accepted February 25, 2014*)

Stealth is a frequent requirement in military applications and involves the use of devices whose signals are difficult to intercept or identify by the enemy. The silent sonar concept was studied and developed at the Department of Marine Electronic Systems of the Gdansk University of Technology. The work included a detailed theoretical analysis, computer simulations and some experimental research. The results of the theoretical analysis and computer simulation suggested that target detection and positioning accuracy deteriorate as the speed of the target increases, a consequence of the Doppler effect. As a result, more research and measurements had to be conducted to verify the initial findings. To ensure that the results can be compared with those from the experimental silent sonar model, the target's actual position and speed had to be precisely controlled. The article presents the measurement results of a silent sonar model looking at its detection, range resolution and problems of incorrect positioning of moving targets as a consequence of the Doppler effect. The results were compared with those from the theoretical studies and computer simulations.

Keywords: silent sonar, wideband signal, detection, distance measurements, accuracy.

1. Introduction

Ideally, submarines, underwater vehicles and divers conducting military operations should be impossible for the enemy to detect. This objective, however, has never been fully realised thanks to active and passive sonars and underwater surveillance systems such as the SOSUS (Friedman, 2006) aboard ships, aircraft and helicopters. Efforts to inhibit underwater traffic detection (mainly submarines) are designed to reduce target strength in the case of active sonar and the power of acoustic signals in the case of passive sonar. The signals are generated by the ship's screw propeller, hull vibrations and non-laminar flow of water around the hull. Used by submarines and underwater vehicles for surveillance and navigation, active sonars are a special source of acoustic signals. The sounding signals which they emit may be detected by intercept sonars (Waite, 2002; Hodges 2010) aboard enemy ships, a clear sign of underwater traffic. By analysing the sounding signals from the intercept sonar we can identify signal parameters and consequently the sonar type. With intercept systems capable of providing target bearing, the risk of exposure becomes even higher.

While radiolocation experiences similar problems, they may be overcome with Low Probability of Intercept Radars (Pace, 2009) (silent radar) which operate on a continuous wave with frequency modulation (CW FM radar). The signals emitted by such a radar have very low power which makes their detection more difficult and increases detection distance. Using radiolocation solutions as a model (Fuller, 1990; Griffiths, 1990; Skolnik, 2008; Levanon, Mozeson, 2004) efforts were taken to build silent sonar. This is supported by the need to ensure submarine and underwater vehicle stealth and the fact that new advanced signal processing methods are available for obtaining the required sonar parameters. In addition, to ensure stealth, submarines do not use sonar which increases the risk of collision with navigational obstacles.

The reason why silent sonar is not commonly used is the Doppler effect with its negative impact on acoustic signal detection and accuracy of target positioning (Marszal, Salamon, 2012a). In addition, the strong absorption coefficient of acoustic wave in water (especially on higher frequencies) means that the signal detection range is naturally limited (Salamon, Marszal, 2013).

There are two basic criteria that silent sonar should meet, i.e. its operating parameters (range, accuracy of target positioning, resolution) should be comparable with those of conventional pulse sonar and its sounding signal should be difficult for the enemy's intercept sonar to detect. The first criterion is met by high energy and narrow auto-correlation function sounding signals. The second criterion may be met if the sounding signal is realistically not known to the surveillance system. Signals with unknown parameters on the white noise background are best detected using the energy detector (Lathi, Ding, 2010), which compares the energy of the signal as it is received in subsequent time intervals. The detector is most effective in the case of pulse sounding signals because some time intervals include noise only while others pick up noise along with a sounding signal. This suggests that silent sonar signals should be continuous. The energy of the received signal is proportional to its power (sound intensity). As a result, the likelihood that a surveillance system will detect the signal will be lower if silent sonar emits a lower power sounding signal. If the surveillance system uses energy detectors with narrowband filters before them, detection may be based on comparing the energies in the particular frequency bands. It will be inhibited, if the sounding signal has a wide spectrum. Broadband signals are also difficult to detect in intercept sonars conducting spectral analysis of the signals received (McDonough, Whalen, 1995). To sum up, silent sonar should emit a continuous signal with a broad spectrum. Sonars which achieve broad spectra through the use of frequency modulation signals have been known for more than fifty years; they are Continuous Wave Frequency Modulation (CW FM) sonars (Kay, 1959; 1960). Recent years have seen more development work on Continuous Active Sonar (CAS) which is designed to ensure continuous target observation especially using long-range sonars (vanVossen *et al.*, 2011; Stove 1992). Conventional long-range Pulsed Active Sonars (PAS) emit the sounding signal every fifty seconds or so which renders a possibly very inaccurate position of moving targets. The design of CAS is based on the intention to reduce the time between target detection moments; the lower sounding signal power is merely a side effect. For short durations of surveillance, the Doppler effect only has a minimal impact and is not analysed in detail as a result. Unlike these sonars, silent sonar must resolve the problem of power emitted and deal with the impact of the Doppler effect on its system design (Marszal *et al.*, 2011; Marszal, Salamon, 2012a; Salamon *et al.*, 2011a).

Developed at the Department of Marine Electronic Systems of the Gdansk University of Technology, the silent sonar concept has been theoretically verified and confirmed using computer simulation and some early experiments with the sonar model (Salamon, Marszal, 2013).

2. Design, principle of operation and parameters of silent sonar

The measurement results presented below come from a silent sonar model which has all the relevant elements of a real life system that determine its basic parameters. In addition, we will assume that the sonar operates in an unlimited, homogenous and lossless medium. Figure 1 shows the silent sonar block diagram.

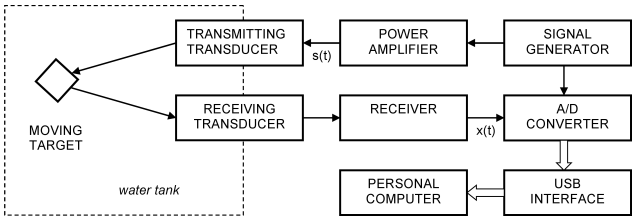

Fig. 1. Block diagram of experimental silent sonar model.

The signal generator generates a continuous, periodical signal $s(t)$ of duration T which can be written as:

$$s(t) = \sum_{m=1}^{\infty} f(t - mT). \tag{1}$$

Each successive period contains signal $f(t)$ with linear frequency modulation (LFM) or hyperbolic frequency modulation (HFM). The LFM signal is described with the function:

$$f_l(t) = \sin\left[2\pi\left(f_0 - \frac{B}{2} + \frac{B}{2T}t\right)t\right], \quad 0 < t < T, \tag{2}$$

where f_0 is the carrier frequency, and B – the width of signal spectrum.

The HFM signal is described with the formula:

$$f_h(t) = \sin\left[2\pi\left(\frac{f_0^2}{B} - \frac{B}{4}\right)T\ln\left(1 - \frac{2B}{(2f_0 + B)T}t\right)\right], \quad 0 < t < T. \tag{3}$$

Signal $s(t)$ is radiated by the transmitting transducer, reflected off a target at distance R_0, and received by the receiving transducer installed next to the transmitting transducer and then amplified. Because the experimental sonar model's distance between the target and transducers is small, the amplitude X_0 of the signal received $x(t)$ depends on the distance R_0 only and remains constant if the target is motionless. Consequently, signal $x(t)$ is a delayed and smaller copy of the signal transmitted which can be written as:

$$x(t) = X_0 s(t - \tau), \tag{4}$$

where $\tau = 2R_0/c$, and c is the speed of acoustic wave propagation in water.

Signal $x(t)$, following sampling with frequency f_s and transformation into digital form is recorded in

computer memory as a discreet signal $x(n)$, where $n = 1, 2, ..., N$, and $N = \mathrm{Ent}(Tf_s)$. Detection is performed in the computer. One of the detection methods that can be used in CWFM systems is matched filtration (Marszal, Salamon, 2013). Applied to silent sonar (Salamon *et al.*, 2011a), the method involves calculating discreet Fourier transforms of a single transmitted signal duration $s(n)$, i.e. the functions $f_l(n)$ or $f_h(n)$. The transforms are stored in computer memory and used for further calculations. As time progresses, a successive calculation is made of discreet Fourier transforms of the signal received $x(n)$ in time intervals $[mT, (m+1)T]$. It is important to observe that each of the intervals includes the final fragment of the previous signal duration and the initial fragment of the current duration as illustrated in Fig. 2. Despite this, the discreet spectrum of the signal received $X(k)$ in each of the intervals has the following form:

$$X(k) = X_0 \exp\left[-j(k-1)n_0/N\right] F(k),$$
$$k = 1, 2, ..., N, \tag{5}$$

where $n_0 = \mathrm{Ent}(\tau f_s)$, and $F(k)$ is the discreet transform of signal $f_l(n)$ or $f_h(k)$. This is the result of a

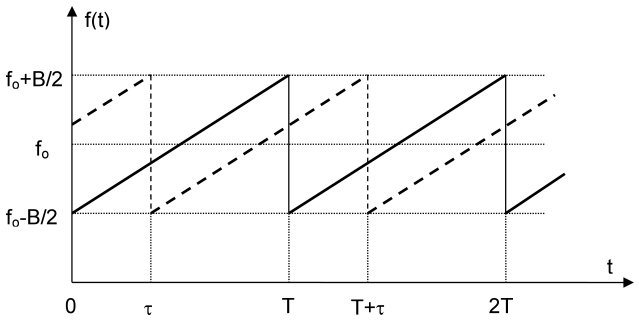

Fig. 2. The frequencies of the signal transmitted (solid line) and echo signal (broken line).

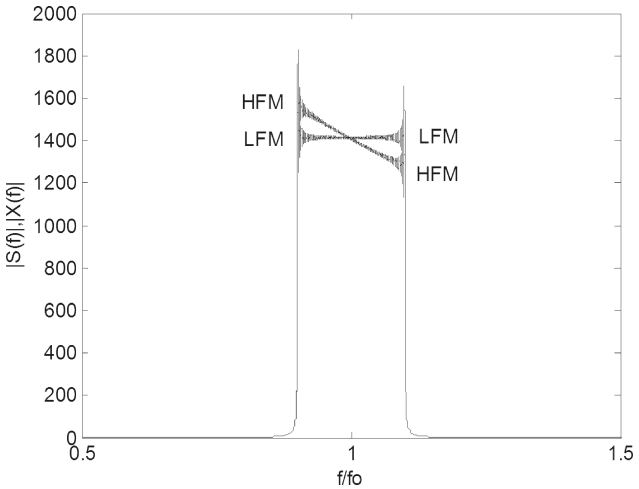

Fig. 3. Spectral modules $S(f) = X(f)$ of signals with frequency modulation: linear LFM and hyperbolic HFM modulation ($f_0 = 10$ kHz, $B = 2$ kHz, $T = 10$ s, $f_s = 40$ kHz, $X_0 = 1$).

property of discreet Fourier transformation of periodical signals when the time duration used for calculating the transform is equal to the signal duration (Lathi, Ding, 2010; Hodges, 2010). The numerically determined modules of the spectra of the signal transmitted $S(f)$ and received $X(f)$, as shown in Fig. 3 are indiscernible. To distinct the two, they are shown as the continuous frequency function.

The next step is to conduct operations described with the following formula:

$$y(n) = \Im^{-1}\{F^*(k)X(k)\}, \tag{6}$$

where the asterisk is used to mark the function conjugated in relation to $F(k)$.

By inserting relation (5) into the formula and using the known properties of the Fourier transform, we obtain:

$$y(n) = X_0 r_{ff}(n - n_0), \tag{7}$$

where $r_{ff}(n)$ denotes the signal auto-correlation function $f_l(n)$ or $f_h(n)$.

In terms of sonar parameters, the ones that matter are signal $y(n)$ maximum, its position on the time axis, main lobe width and side lobe level.

Figure 4 shows a numerically determined echo signal $y(t)$ from a target at distance $R_0 = 3$ km, received together with white Gaussian noise. As you can see, the output signal maximum occurs at the distance given.

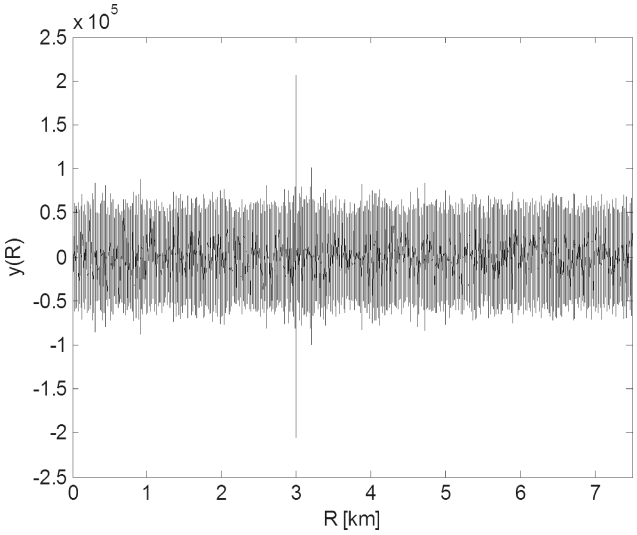

Fig. 4. LFM output signal echo at distance $R_0 = 3$ km ($f_0 = 10$ kHz, $B = 2$ kHz, $T = 10$ s, $f_s = 40$ kHz, $X_0 = 1$, $M = 0.1$).

Scale R in the figure is related to the sample number via relation $R = 0.5 \cdot c \cdot n/f_s$. The only reason why the distance to a motionless target is wrongly calculated is because the sound velocity was wrongly identified. We will discuss errors in calculating the position of moving targets in the next chapter.

In the absence of noise, the maximal value of signal $y(n)$ is $y(n_0) = 0.5X_0N = 0.5X_0Tf_s$, because the

maximal value of the auto-correlation function of signals $f(n)$ is equal to their energy which in this case is $0.5N$. This is the determining factor of the signal to noise ratio which for white Gaussian noise with spectral density $M/2$ is equal to:

$$SNR_0 = \frac{y^2(n_0)}{\sigma^2} = \frac{X_0^2 T}{M}, \tag{8}$$

because the variation of matched filter output noise is equal to $\sigma^2 = 0.25NMf_s$, (Salamon, 2006). In the case of the data used in Fig. 4 ($X_0 = 1$, $T = 10$ s, $M = 0.1$) the output signal to noise ratio is $SNR_0 = 100$. The example shown in the figure has a numerically calculated ratio equal to $SNR_0 = 107$. This is because the effect of noise in this case causes the maximal signal value to increase.

As we can see from formula (8), the desired signal to noise ratio can be achieved by reducing signal power and proportionally extending its duration. Used in silent sonar to reduce the transmitter's power, the method makes sounding signal detection more difficult for intercept sonar. What makes detection in this sonar even more difficult is that the sounding signal is unknown which excludes matched filtration. If applied, matched filtration gains BT times the input signal to noise ratio SNR_i, because $SNR_0 = BT \cdot SNR_i$ (Salamon, 2006). In the example in Fig. 4 the quotient is $BT = 2 \cdot 10^4$, which means that the input signal to noise ratio is $SNR_i = 0.005$.

Figure 5 shows the shape of the envelope of signal $y(t)$ with linear and hyperbolic frequency modulation. The envelopes were determined using Hilbert transform. As you can see, the type of modulation has practically no effect on the signal. Main lobe width between the zeros is $\Delta t = 2/B$, which gives sonar range resolution at $\delta R = c\Delta t/4 = c/2B$. The sonar achieves good resolution by using a broad spectrum of the sounding signal.

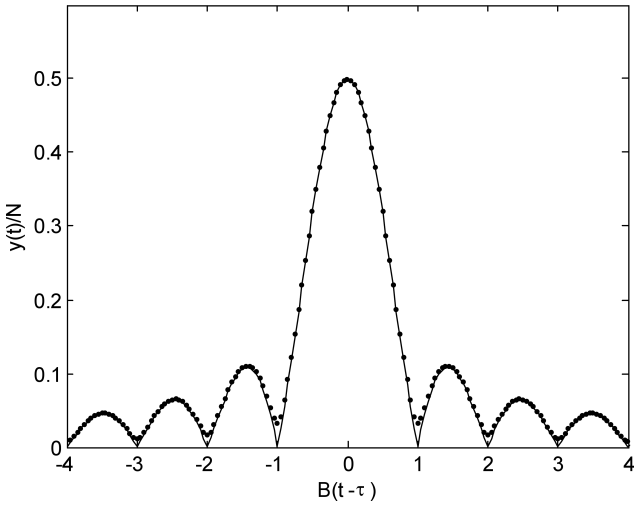

Fig. 5. Fragment of output signals around the maximal value: solid line – LFM signal, dotted line – HFM signal ($R_0 = 3$ km, $\tau = 4$ s, $f_0 = 10$ kHz, $B = 2$ kHz, $T = 10$ s, $f_s = 40$ kHz, $X_0 = 1$, $M = 0$).

3. Moving target detection

While the sonar described above was used to detect a motionless target, the majority of real life applications will be on ships in motion searching for moving targets. This will cause the Doppler effect in echo signal. Its impact on the operation of silent sonar will be discussed below.

Most Doppler effects apply to the sinusoidal signal and are manifested as a change of frequency. If the signal is a pulse, broadband or periodical signal, the Doppler effect may be treated as compression or expansion in time of echo signal (Marszal *et al.*, 2011; Marszal, Salamon, 2012a). If we ignore the insignificant change of amplitude, the signal can then be written as:

$$x_d(t) = X_0 s[d(t - \tau)], \tag{9}$$

where

$$d = \frac{1 + v/c}{1 - v/c} \cong 1 + 2v/c. \tag{10}$$

Velocity v is a so called radial velocity which describes how the distance between target and signal changes over time. If the vector of target velocity $\mathbf{v}$ versus the signal is inclined towards the straight line that connects the target with the signal at angle α, then $v = |\mathbf{v}| \cos\alpha$. We can assume that target velocity is constant during surveillance, and when the target-sonar distance is long, angle α is constant as well. The plus sign of velocity v means that the target is nearing the sonar.

In the case of periodical sounding signals in question, the Doppler effect changes the duration of echo signal T/d. As a consequence, its location and spectral width change, as illustrated in Fig. 6.

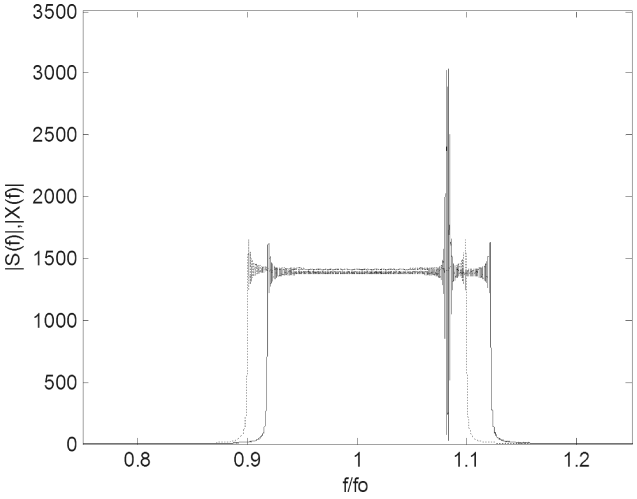

Fig. 6. Spectra of LFM echo signal: solid line – $v = 15$ m/s, dotted line – $v = 0$ m/s ($R_0 = 3$ km, $f_0 = 10$ kHz, $B = 2$ kHz, $T = 10$ s, $f_s = 40$ kHz, $X_0 = 1$, $M = 0$).

The output signal determined from formula (6) is not described with the auto-correlation function of the signal transmitted $r_{ff}(t)$. It is described with the correlation function $r_{fx}(t)$ of signal $f(t)$ with signal $x_d(t)$, described with formula (9). Theoretical calculations suggest (Marszal *et al.*, 2011; Marszal, Salamon, 2012a), that the parameters of the correlation function $r_{fx}(t)$ are worse than those of auto-correlation $r_{ff}(t)$, namely:

- lower maximal values
- greater width,
- its maximum is shifted on the time axis in relation to the actual delay τ.

How the Doppler effect affects the value of the correlation function's maximal value $r_{fx}(t)$ depends on the type of modulation. That effect is significantly lower for HFM signals compared to LFM signals (Kroszczyński, 1969; Yang, Sarkar, 2006).

It can be seen in Fig. 7. This is the reason why detection performance regarding hyperbolic modulation signals is practically independent of the speed of the targets.

The width of the correlation function for LFM signals, which is a decisive factor for sonar range resolution, grows proportional to velocity v. Theoretical analysis (Marszal, Salamon, 2012a) shows that for $v > 0$ the resolution is:

$$\delta R = 2vT. \tag{11}$$

As a result, it is equal to double the distance covered by the target during a single sounding signal duration, as can be seen in Fig. 7a.

In the case of HFM signals, range resolution may be considered as the distance between short pulses, a lower and a higher one, which produce echo signal from a specific target. The distance is about half the distance of LFM signals, as shown in Fig. 7b. The height of the lower pulse drops as the distance to the target is decreasing. However, with the height of the higher pulse increasing, range resolution may improve significantly.

The shift of the correlation function's maximum on the time axis produces inaccurate target distance measurements. Theoretical analysis and numerical calculations show that the error can be described with formula (Marszal, Salamon, 2012a):

$$\Delta R \cong -vT\left(\frac{f_0}{B} + \frac{1}{2}\right), \tag{12}$$

where $\Delta R = c(t_0 - \tau)/2$, t_0 means the moment when the output signal reaches its maximum, and $\tau = 2R_0/c$ is the delay versus the start of the transmitted signal's duration.

The dotted lines in Fig. 7 show the distance measurement errors determined from formula (12). Please note that the distance measurement error does not depend on the target distance. Significant distance measurement errors are a major problem in silent sonar. The methods to limit these errors are described in

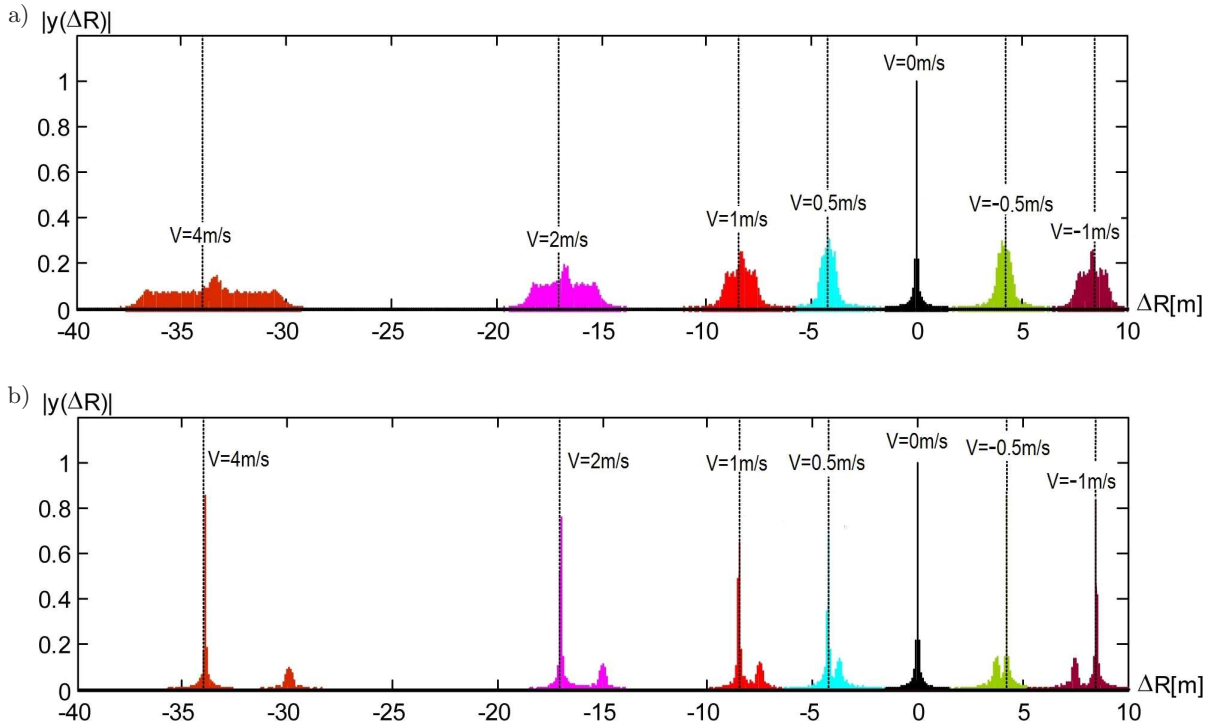

Fig. 7. Error in measuring the distances to moving targets for signals: a) LFM, b) HFM ($R_0 = 100$ m, $f_0 = 160$ kHz, $B = 20$ kHz, $T = 1$ s, $f_s = 720$ kHz, $X_0 = 1$, $M = 0$).

the papers (Salamon *et al.*, 2011b; Marszal *et al.*, 2012b; Marszal, Salamon, 2013).

4. Measurement set

The measurements described below were taken using a set comprising:

- experimental model of silent sonar,
- underwater acoustic target,
- model basin with a mobile and fixed platform.

There is no difference between the block diagrams of experimental and real silent sonar as shown in Fig. 1. The experimental model was built from custom-made sub-assemblies and standard measurement equipment.

The receiving and transmitting transducers are built from PZT ceramics. The transducers' mid-channel frequency is 159.5 kHz with 20 kHz transfer bandwidth, and beam width in both cross-sections equal to about 7°.

The in-house designed power amplifier is a broadband linear amplifier with maximum output voltage 136 V_{pp}, which corresponds to 15 W of power supplied to the transmitting transducer. Because the operation involved broadband signals, no transmitting transducer compensation systems were used. As a result, the radiation efficiency achieved is 10%. With 15 W of power supplied, source level SL_{MAX} is equal to 201 dB Re 1 μPa·m. Supplied to the power amplifier's input are periodical LFM and HFM signals, as described earlier, or ping type pulse signals, as a comparison. They are generated by a Tektronix AFG3011 signal generator.

The echo signals from the receiving transducer are amplified in an in-house designed selective amplifier with mid-channel frequency 159.5 kHz and 20 kHz transfer bandwidth. The amplifier's voltage gain is regulated and reaches the maximum of 140 dB.

Signals from the generator output and receiving amplifier output are sampled at frequency 638 kHz and converted into digital form in a multi-channel 14-bit A/C converter using AD7367 integrated circuits by Analog Devices. Digital signals are sent to a PC computer via USB and recorded on the disk. Stored in files, samples of transmitting and receiving signals with registered distance markers are processed off-line in the MATLAB environment using the algorithms described above.

In addition, to make sure that the measurements are correct, transmitted and received signals can be viewed using an oscilloscope by Agilent Technologies DSO6034A.

The underwater acoustic target is a corner reflector built at the Department of Marine Electronic Systems. Covered with foamed neoprene with closed pores, its side is 16 cm long which corresponds to target strength for operating frequency of 159.5 kHz equal to about 8 dB. Placed in a water-filled streamlined casing (70 cm in length and a diameter of 25 cm), the reflector can move without any turbulence which could falsify the results. The maximal speeds for which this requirement was met were 4 m/s forward and 1 m/s backward. Figure 8 shows a picture of the target and its design.

Fig. 8. The experimental target.

The measurements were taken at the Gdansk-based Ship Design and Research Centre (Centrum Techniki Okrętowej S.A.), a facility usually used for testing ship models. The model basin is 270 m long, 12 m wide and 5.5 m deep. You can see it in Fig. 9. The basin has a smooth concrete structure and no acoustic wave absorption. Both ends of the pool have a shallower bottom covered with stones. The sides halfway through the pool have surface wave breakers.

Fig. 9. Model basin (with a mobile towing carriage in the background).

Because all the other walls and bottom of the pool are smooth, the reflections of acoustic wave are mirror reflections and the backscattering level is low. As a result, for distances between 60 m to 130 m surface reverberation is low. Based on this, it was agreed that the range of distances meets the requirements of the investigation.

The towing carriage (seen in the background in Fig. 9) runs on rails attached to the sides of the basin. It moves above water surface with a pre-determined and carefully controlled speed. The target is fixed to the carriage on a pipe with a guy rope. Target draught was 2.5 m. Figure 10 shows a picture of the target mounted to the carriage platform as it is moving at 4 m/s. Attached to the other platform, which is fixed, are a transmitting and a receiving transducer of the sonar model. They are 2.5 m below water surface. To ensure that the target can be precisely located as the carriage is moving, the measurement files are also recording its momentary speed and markers on the time axis generated at 80 m and 100 m away from the ultrasound transducers. The markers are generated when the shutters, placed along the edge of the pool, align with the slotted optical switch attached to the edge of the towing carriage.

Fig. 10. View of the experimental underwater acoustic target mounted on the mobile platform while being measured at a speed equal to 4 m/s.

5. Measurement method and results

The objective of the measurement was to confirm experimentally the results of the theoretical analysis and numerical simulation tests of silent sonar presented in the previous chapters. The measurements were taken in two cycles, for a motionless target and a target moving at a given speed. The first measurement cycle included 42 measurement series for the motionless target and different parameters of the sounding signal. The second measurement cycle included 78 measurement series for a variety of sounding signal combinations and different target speeds.

Prior to the start of the measurements, the constant echoes were studied to help select a range of distances for the purpose of the measurements. Based on this, an area was selected within a range of 50 m and 130 m from the ultrasound transducers, where constant echoes are very weak. The objective of the initial part of the first measurement cycle was to study the effect of sounding signal types on resolution and the shape of echo signal from a motionless target for ping, LFM and HFM sounding signals. In this measurement series the motionless target was 80 m away from the sonar's transducers on their acoustic axis. The transmitter was emitting a ping type pulse signal with frequency $f_0 = 159.5$ kHz and duration $t_i = 100$ µs. The width of the main lobe of the signal's spectrum was $B_i = 20$ kHz. HFM and LFM signals emitted by the transmitter had the same mid-channel frequency and spectral widths, which should ensure a similar range resolution of pulse and broadband signals. Input noise levels were also guaranteed to be the same when receiving both types of signal, when the receiver's transfer band was 20 kHz. The maximal voltage on the transmitting transducer for pulse signal was $V_i = 27V_{pp}$, which corresponded to power $P_i = 0.58$ W and source level $SL_i = 187$ dB/Re 1µPa·m. In the case of continuous LFM and HFM signals, the voltage was equal to $V_{FM} = 4.6V_{pp}$, which corresponded to power $P_{FM} = 17$ mW and source level $SL_{FM} = 171$ dB/Re 1µPa·m.

Figure 11 shows the echo signal from a motionless target for a ping type pulse signal with duration $t_i = 100$ µs. The amplitude of the signal shown in the figure was normalised in relation to the maximal value of the echo from the target. The range of the distance of 250 m covers the entire length of the basin. Apart from the echo signal from the target at a distance of 80 m, constant echoes from the basin's structure can also be seen. They will appear in the other figures as

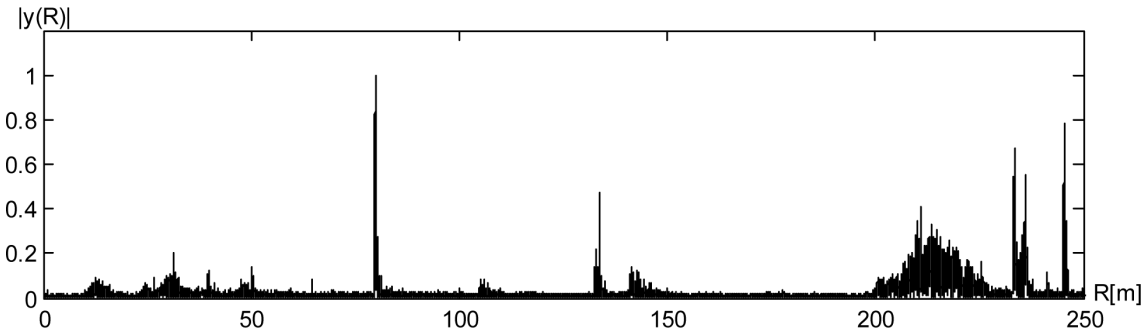

Fig. 11. Normalised echo signal from a motionless target (80 m away) in the background of constant echoes. Sounding signal ping 0.1 ms, range of distances 250 m.

well but will not be commented on. For analogous measurements with LFM and HFM type sounding signals, normalised echo signals after correlation detection for a full range of distances 250 m are not distinguishable from those in Fig. 11.

Figure 12a shows a zoomed in fragment of the envelope of echo signal from Fig. 11 within a distance of 80m, which includes the echo from the hydroacoustic target. As you can see, the echo signal envelope has several maxima and the total echo duration corresponds to a length of about 76 cm, which is significantly higher than the resolution for a fixed target equal to $\delta R = ct_i/2 = 7.5$ cm. This is due to the target design shown in Fig. 8 whose components (copula of the casing, pipe, corner reflector) are independent sources of the reflected wave. The other phenomenon affecting the echo shape is multipath propagation which is the result of basin design. As an example, the path (towards the target) of a signal reflected off the water surface differs from the direct path by 16 cm, and by 24 cm if reflected off the bottom.

Figure 12b shows the echo signal envelope for an LFM type sounding signal with duration $T = 1$ s and bandwidth $B = 20$ kHz. Figure 12c, on the other hand, shows an analogous situation for an HFM type of signal. The resolutions of echoes in figures a), b) and c) are similar. In the case of LFM and HFM sounding signals there is a shape blur of the echo as a result of the side lobes of the auto-correlation function (sinx/x type) of the sounding signal with frequency modulation.

Because the echo is blurred and repeated multiple times due to the design of the target and propagation

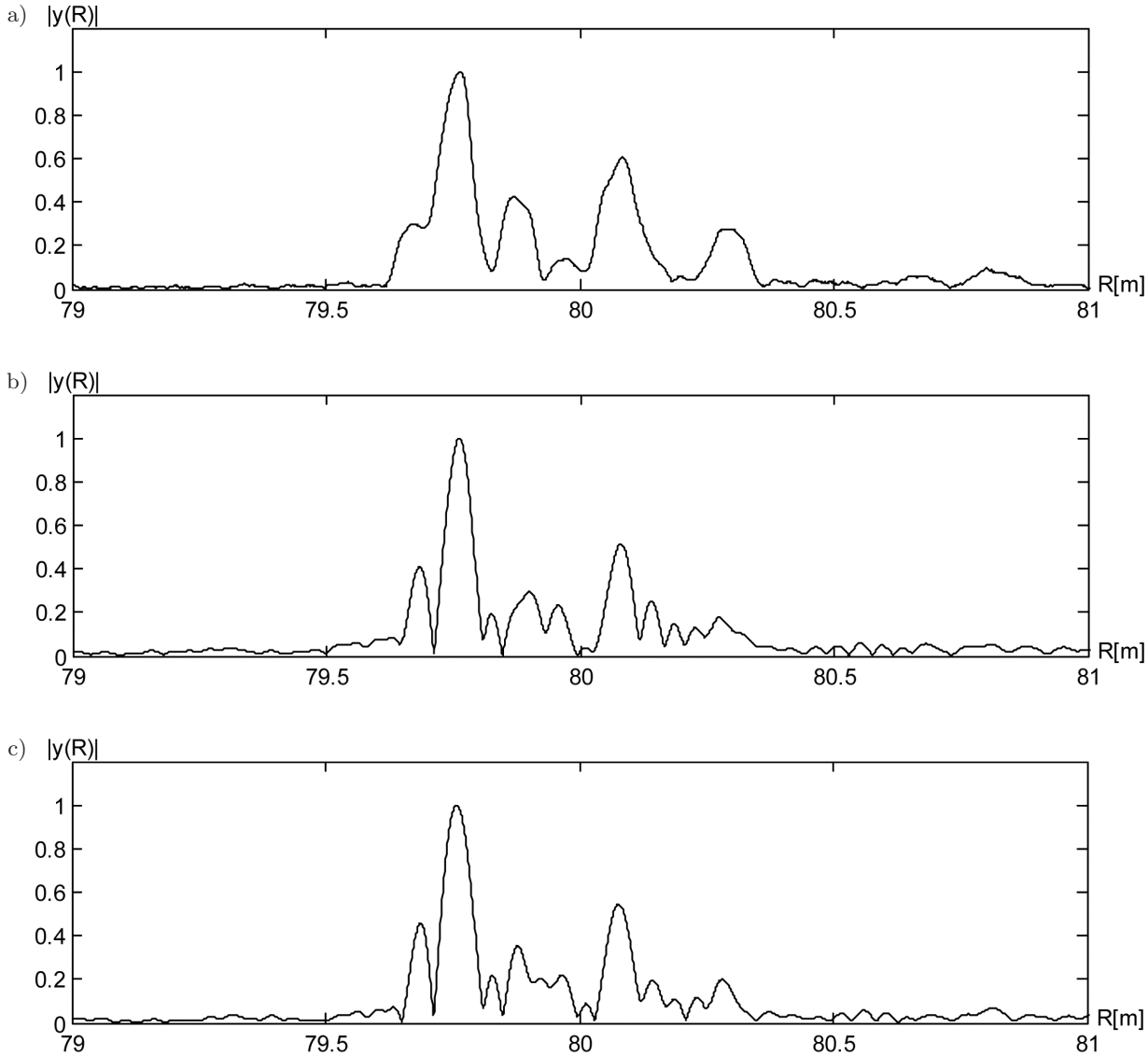

Fig. 12. Envelope of echo signal from a target for sounding signals: a) ping type $t_i = 100$ µs; b) LFM type $B = 20$ kHz, $T = 1$ s; c) HFM type $B = 20$ kHz, $T = 1$ s.

conditions in the basin, it is not possible to conduct a detailed analysis of the effect of sounding signal parameters on sonar range resolution. What the data show, however, is that sonar resolution is not much different from the theoretical resolution illustrated in Fig. 5.

The next series of measurements involving a motionless target, studied the possibility of reducing silent sonar signal power compared to the power emitted by pulse sonar. The objective of the measurements was to compare the signal to noise ratio for a sounding made with a ping type pulse with parameters as described above ($t_i = 100$ µs, $P_i = 0.58$ W, $SL_i = 187$ dB/Re 1 µPa·m) and continuous LFM and HFM signals with a band equal to 20 kHz and durations equal to $T = 0.5$ s, 1 s, 2 s and 4 s. The power of LFM and HFM signals was changed from 17 mW ($SL = 171$ dB/Re 1 µPa·m) to 5 µW ($SL = 136$ dB/Re 1µPa·m). Figure 13 shows a comparison of a normalised echogram for a pulse signal described above (Fig. 13a) with normalised echograms for LFM signals, transmitter power 5 µW ($SL = 136$ dB/Re 1 µPa·m), band $B = 20$ kHz and processing intervals equal to $T = 0.5$ s (Fig. 13b) and 4 s (Fig. 13c). Because the transmitted signal level was so low, the echo signal at receiver input was below the noise level. Table 1 shows the parameters of comparable signals and the values of the received correlational signal to noise ratio. The real effective noise voltage was calculated numerically (Webster, 1999) based on samples recorded for a ping type sounding signal and for frequency modulation sounding signals, additionally undergoing matched filtration. The processing gain was calculated using this relation:

$$PG_k = SL_0 - SL_k + SNR_k - SNR_0, \qquad (13)$$

where PG_k means Processing Gain for k-th sounding signal, SL_0 – source level for ping type signal, SL_k – source level for k-th sounding signal, SNR_k signal to noise ratio for k-th sounding signal, SNR_0 – signal to noise ratio for ping type signal.

The objective of the second measurement cycle was to understand the effect of target speed on detection performance and positioning accuracy. The transmitting transducer input was receiving continuous LFM and HFM sounding signals. Their parameters varied each time. At the same time the target was moving within the transducers' acoustic axis at different speeds. Echo signals from the receiver output and sounding signals and distance markers were recorded in measurement files for further off-line processing. All measurements were taken for an identical level of the transmitting signal equal to $V_{FM} = 4.6$ V_{pp}, which corresponded to power $P_{FM} = 17$ mW and source level $SL_{FM} = 171$ dB/Re 1 µPa·m. The width of LFM and HFM signal spectrum was $B = 20$ kHz or $B = 10$ kHz and the frequency modulation direction was up or down (chirp up, chirp down). Modulation time was $T = 0.5$ s, 1 s, 2 s and 4 s. The speeds selected for the target were: $v = -05$ m/s, -1 m/s, 1 m/s, 2 m/s and 4 m/s. Distance markers were sent when the target was 100 m and 80 m away from ultrasound transducers.

The measurement data were used to develop synthetic comparisons to help understand how the parameters of sounding signal and target speed affect detection and accuracy of distance measurements. Figure 14 shows the relation between errors in measuring distance ΔR and target speed for a sounding signal with band $B = 20$ kHz and duration equal to $T = 1$ s LFM signals (Fig. 14a) and HFM signal (Fig. 14b). The figures were made by superimposing the echograms of different target speeds. The individual echograms were normalised in relation to the amplitude of the echo from a motionless target. The zero on the scale corresponds to the real distance between the target and transducers equal to 100 m. As you can see in the figures, the amplitude of echo signal for LFM signals decreases as target speed increases, but stays at a similar level for HFM signals irrespective of target speed.

Table 1. Parameters of sounding signals which produced the echograms in Fig. 13.

k	Signal Pattern	Input Power	Source Level Re 1 µPa·m [dB]	Output SNR [dB]	Obtained Processing Gain [dB]	Theoretical Processing Gain [dB]
0	Ping 100 µs	583 mW	186.7	42.5	0	0
1	LFM 20 kHz, 0.5 s	4.86 µW	135.9	30.3	38.6	40
2	HFM 20 kHz, 0.5 s	4.86 µW	135.9	29.7	38.0	40
3	LFM 20 kHz, 4 s	4.86 µW	135.9	39.9	48.2	49
4	HFM 20 kHz, 4 s	4.86 µW	135.9	39.8	48.1	49

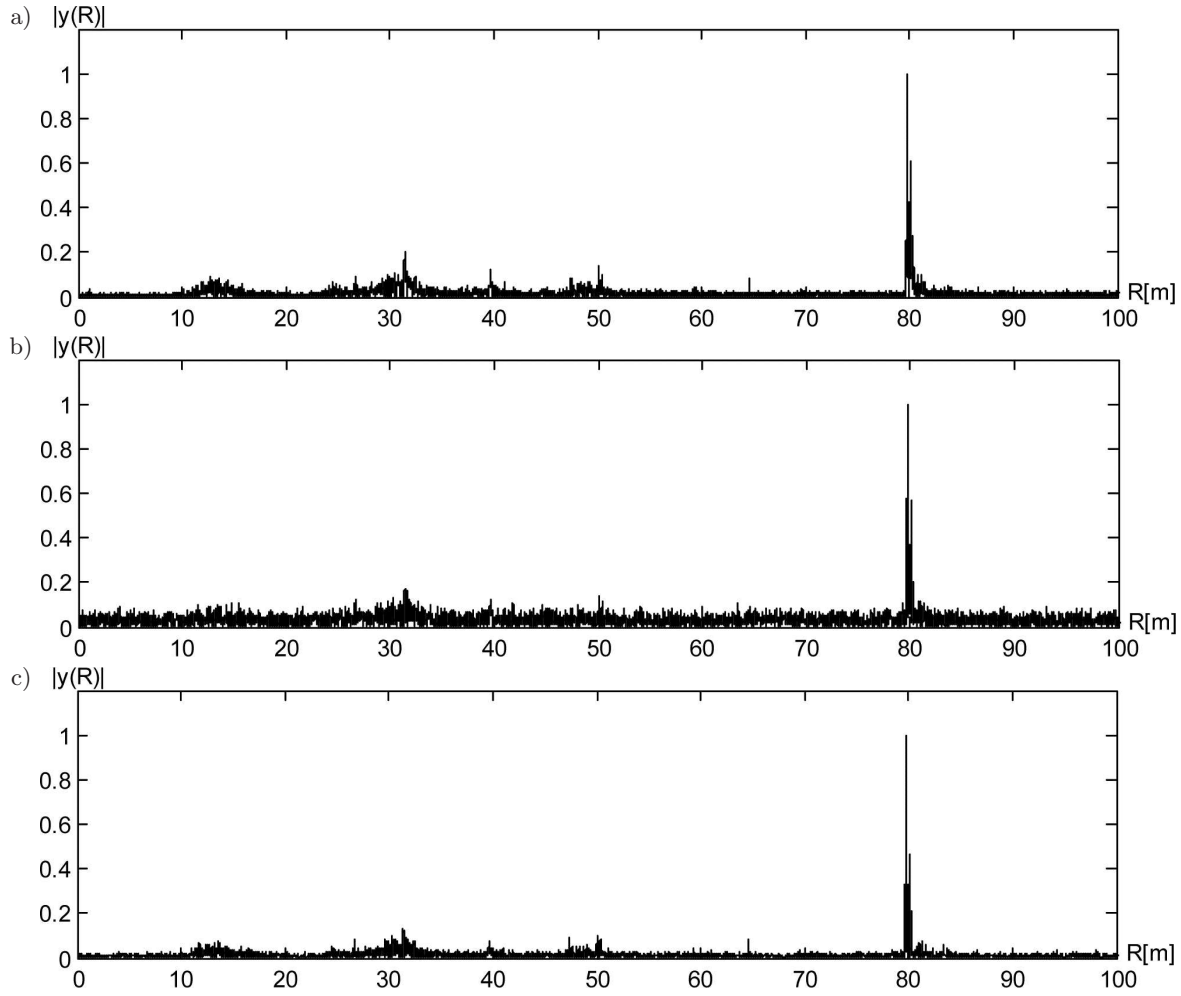

Fig. 13. Normalised echo signal from the motionless target: a) for a ping type sounding signal $t_i = 100$ µs, $SL = 187$ dB, b) for an LFM type sounding signal – $B = 20$ kHz, $P = 5$ µW, $SL = 136$ dB for $T = 0.5$ s, c) as before for $T = 4$ s.

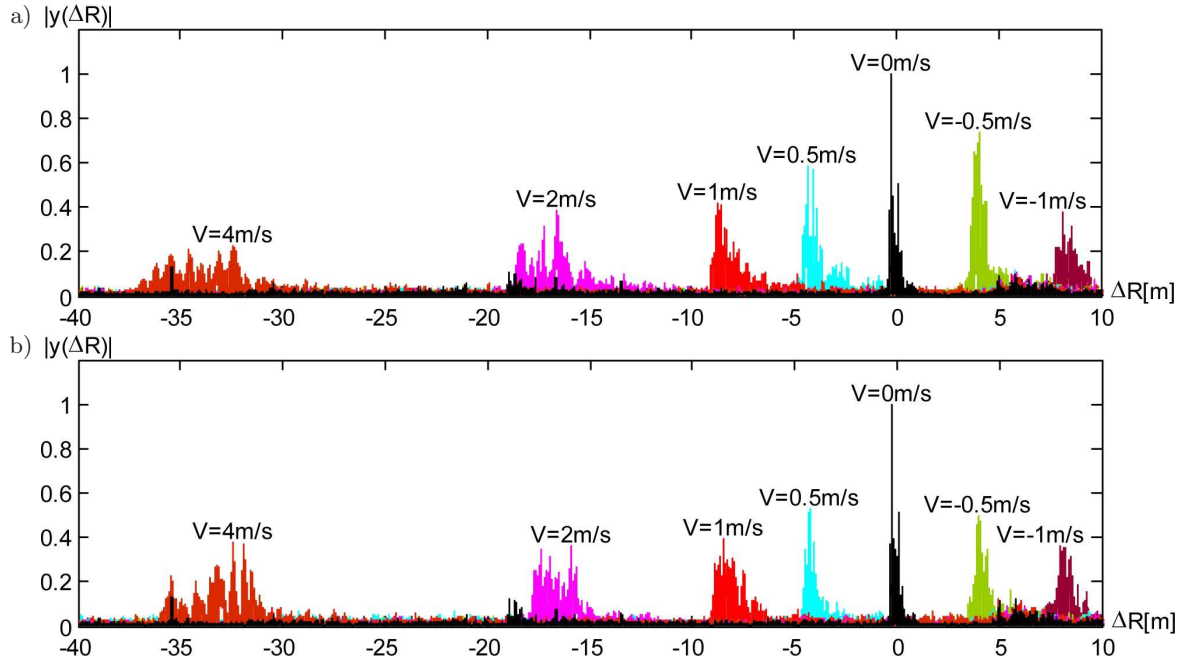

Fig. 14. Error in measuring the distances for various target speeds for sounding signals in the band $B = 20$ kHz and duration $T = 1$ s: a) for an LFM type signal, b) for an HFM type signal.

Just as in Fig. 14, Fig. 15 shows the effect of modulation period duration T on detection and accuracy of target distance measurement. Figure 16, on the other hand, shows the effect of modulation band width on detection and accuracy of distance measurement. The results presented in Figs. 14, 15 and 16 are consistent with the results of the theoretical analysis and simulations shown in Fig. 7.

The measurements also looked at the effect of change in direction of frequency modulation on errors in distance measurements. The result of the measurements for "downward" frequency modulation LFM and HFM type for modulation band 20 kHz and duration equal to 1s is shown in Fig. 17. As expected the error in measuring the distance in this case has a sign opposite to the "upward" frequency modulation.

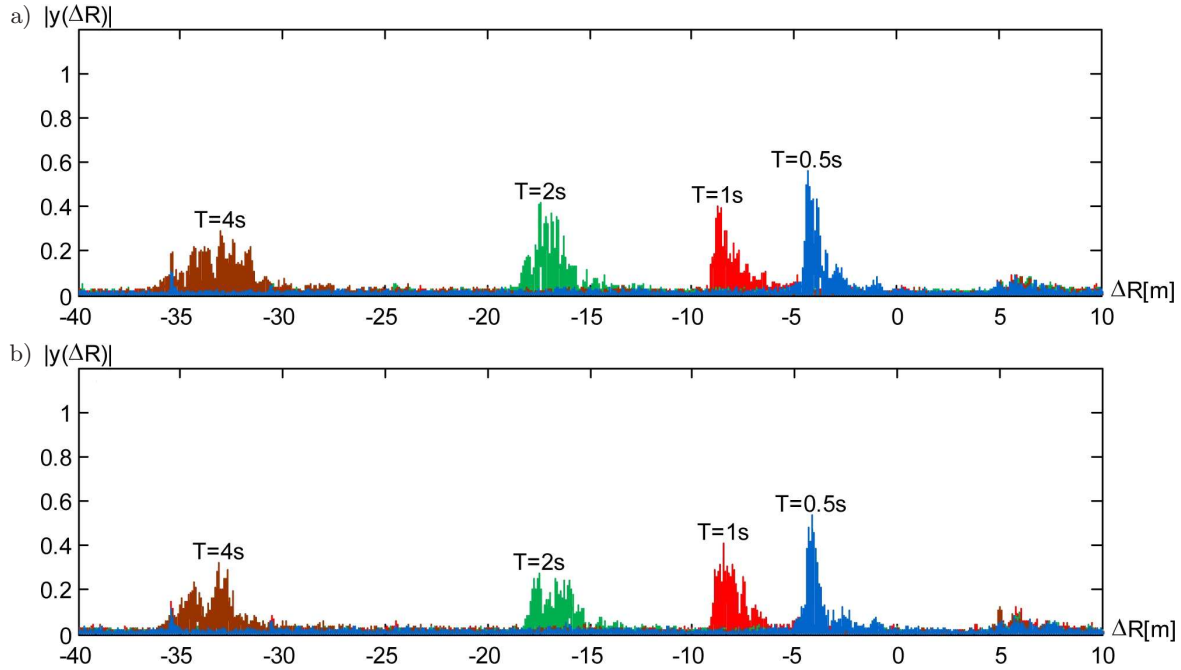

Fig. 15. Error in measuring the distances for various period durations T for sounding signals with band $B = 20$ kHz for target speed $v = 1$ m/s: a) for an LFM type signal, b) for an HFM type signal.

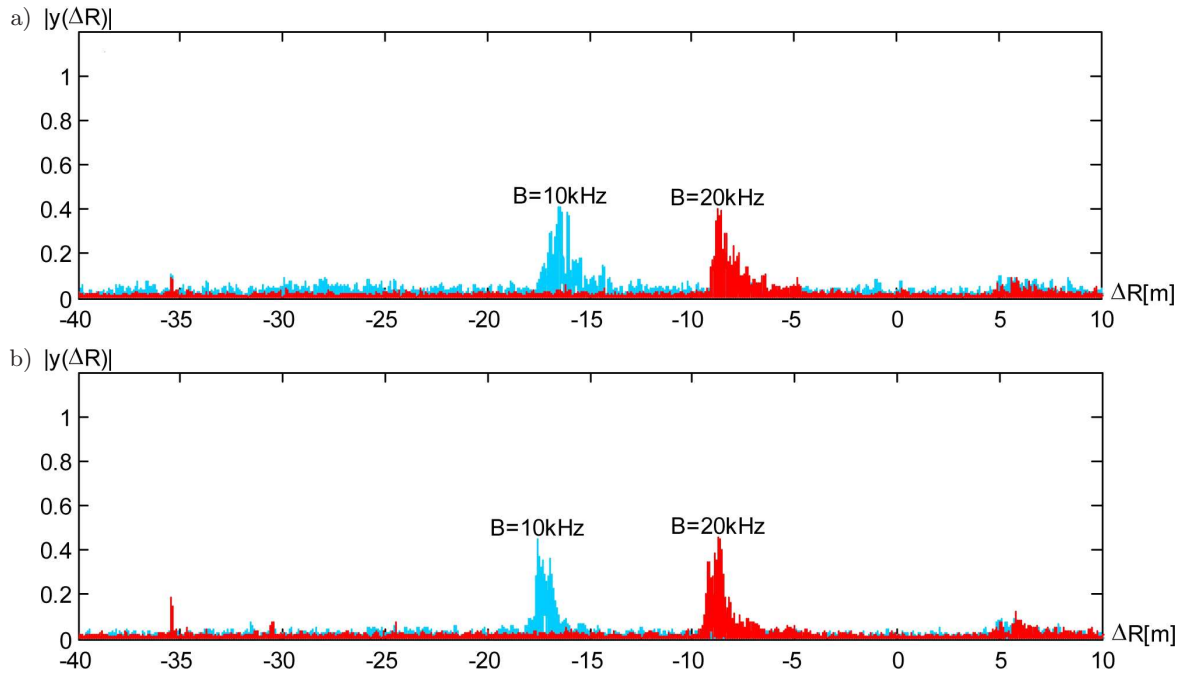

Fig. 16. Error in measuring the distances for various bandwidths of sounding signals for target speed $v = 1$ m/s: a) for an LFM type signal, b) for an HFM type signal.

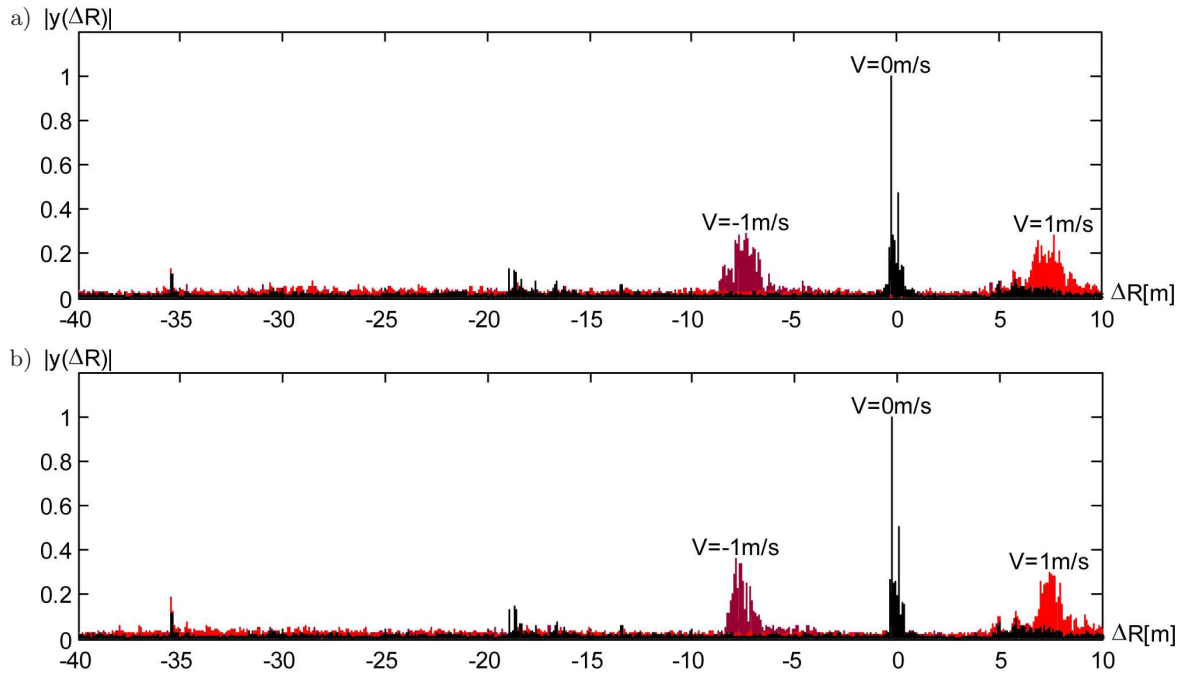

Fig. 17. Error in measuring the distances for Chirp Down $B = 20$ kHz, $T = 1$ s for signals: a) LFM type, b) HFM type.

6. Summary

The silent sonar investigation has fully confirmed the assumptions and the results of theoretical analysis and computer simulations. In particular, it validated claims that when silent sonar uses continuous periodical signals with frequency modulation as sounding signals and echo signal correlational detection on the receiving side, the sounding can be conducted with very low transmitting power.

The experiment has confirmed that when such sounding signals are used for detecting moving targets, the result is poorer detection and errors in distance measurement. It has been confirmed that when the sounding signal uses hyperbolic frequency modulation, detection is less sensitive to the Doppler effect compared to linear frequency modulation. Using relation (12) determined in previous theoretical works (Marszal *et al.*, 2011; Marszal, Salamon, 2012a), we can make a precise calculation of the error in the distance to a moving target using silent sonar with continuous and periodical LFM and HFM sounding signals. This relation is right for targets that are both approaching and moving away as well as for ascending and descending frequency modulation directions.

With the measurement results confirming the occurrence of distance measurement errors, the author firmly believes that more work should be conducted searching for signals that are less sensitive to this effect (Salamon *et al.*, 2011b; Marszal *et al.*, 2012b; Marszal, Salamon, 2013). Despite the error in measuring target distance, the experiment has confirmed other positive features of silent sonar, making it an attractive option in all applications where stealth is a priority.

References

1. Friedman N. (2006), *The naval institute guide to world naval weapon systems*, Naval Institute Press.
2. Fuller K.L. (1990), *To see and not be seen*, IEE Proceedings-F, **137**, 1, 1–10.
3. Griffiths H.D. (1990), *New ideas in FM Radar*, Electron. Commun. Eng. Journal, **2**, 5, 185–194.
4. Hodges R.P. (2010), *Underwater Acoustics: Analysis, Design and Performance of Sonar*, John Wiley & Sons, Ltd.
5. Kay L. (1959), *A comparison between pulse and frequency-modulation echo-ranging system*, J. Brit. IRE, **19**, 2, 105–113.
6. Kay L. (1960), *An experimental comparison between pulse and frequency-modulation echo-ranging system*, J. Brit. IRE, **20**, 10, 785–796.
7. Kroszczyński J.J. (1969), *Pulse compression by means of linear-period modulation*, Proc. IEEE, **57**, 7, 1260–1266.
8. Lathi B.P., Ding Z. (2010), *Modern digital and analog communication systems*, Oxford University Press, New York.
9. Levanon N., Mozeson E. (2004), *Radar signals*, John Wiley & Sons.
10. McDonough R.N., Whalen A.D. (1995), *Detection of Signals in Noise*, (2 ed), Academic Press.

11. Marszal J., Salamon R., Zachariasz K., Schmidt A. (2011), *Doppler effect in CW FM sonar*, Hydroacoustics, Gdańsk, **14**, 157–164.

12. Marszal J., Salamon R. (2012a), *Distance measurement errors in silent FM-CW sonar with matched filtering*, Metrol. Meas. Syst., **XIX**, 2, 321–332.

13. Marszal J., Salamon R., Kilian L. (2012b), *Application of maximum length sequence in silent sonar*, Hydroacoustics, Gdańsk, **15**, 143–152.

14. Marszal J., Salamon R. (2013), *Silent Sonar for Maritime Security Applications*, Proceedings of Meetings on Acoustics, Acoustics Society of America, **17**, 070082.

15. Pace P.E. (2009), *Detecting and Classifying Low Probability of Intercept Radar* (2 ed.), Artech House.

16. Salamon R. (2006), *Sonar systems* [in Polish], Gdańskie Towarzystwo Naukowe, Gdańsk.

17. Salamon R., Marszal J., Schmidt J., Rudnicki M. (2011a), *Silent sonar with matched filtration*, Hydroacoustics, Gdańsk, **14**, 199–208.

18. Salamon R., Marszal J., Kilian L., Jedel A., Raganowicz A., Ostrowski Z. (2011b), *Choice of the signals in silent sonar with matched filtration* [in Polish], Proceedings of 58th Open Seminar on Acoustics, Gdańsk – Jurata, **2**, 257–266.

19. Salamon R., Marszal J. (2013), *Estimating Intercept Range of Silent Sonar*, in Hydroacoustics of Shallow Water edited by E. Kozaczka, G. Grelowska, Polish Academy of Sciences Institute of Fundamental Technological Research, Warszawa, 139–158.

20. Skolnik M. (2008),*Radar Handbook*, Third Edition, McGraw-Hill Professional.

21. Stove A.G. (1992), *Linear FMCW Radar Techniques*, IEE Proceedings-F, **139**, 5, 343–350.

22. Vanvossen R., Beerens S.P., Vanderspek E. (2011), *Anti-Submarine Warfare With Continuously Active Sonar*, Sea Technology, **52**, 11, 33–35.

23. Waite A.D. (2002), *Sonar for Practising Engineers, Third Edition*, John Wiley & Sons.

24. Webster J.G. (1999), *The Measurement, Instrumentation, and Sensors Handbook*, Springer.

25. Yang J., Sarkar T.K. (2006), *Doppler-invariant property of hyperbolic frequency modulated waveform*, Microwave and optical technology letters, **48**, 8, 1174–1179.